Pattern formation in the Holling-Tanner predator-prey model with predator-taxis. A nonstandard finite difference approach

Heather Banda, Michael Chapwanya* and Phindile Dumani
Department of Mathematics & Applied Mathematics, University of Pretoria, Pretoria 0002, South Africa

Abstract

A characteristic feature of living organisms is their response to the environment in search for food or reproduction opportunities. This paper is devoted to the investigation of the pattern formation of the Holling-Tanner predator-prey model with predator-taxis. We first summarise the qualitative properties of the model where a threshold for the appearance of pattern formation is specified. Then we design and analyse a coupled nonstandard finite difference and finite volume scheme for the proposed model. Numerical simulations are provided to support theoretical findings.

1 Introduction

The pioneering work of Lotka [21] and Voltera [33] on predator-prey systems gave rise to rich literature on biological models on interactions involving two or more species with application to ecology and biology. However, the Lotka-Volterra model has many limitations. It is assumed that when prey multiply, they will have an unlimited food supply and reproduce exponentially unless subject to predation. Another limitation is, in the absence of predators, prey population grows exponentially towards infinity due to the unlimited food supply assumption. While the principles of this model have remained valid until today, there have been improvements on the Lotka–Volterra model, and notables are: Solomon model [27], Rosenzweig–MacArthur model [26], Holling model [13], to name just a few. In this work, we assume the kinetic dynamics of the system is given by the generalised Holling–Tanner predator-prey model, first studied in [30].

Generalised reaction diffusion predator-prey models with self diffusion have been investigated extensively in the literature, see for example [19] and the literature there in. In [19], the authors showed the existence of Hopf bifurcation and Turing instability in the Holling–Tanner model with linear and self diffusion. Predator-prey reaction diffusion models with prey-taxis have been studied extensively in the literature [14, 3, 15, 31, 18, 28, 34, 38], where global existence, dynamic behavior and steady states have been considered. These are strongly coupled models simulating prey avoiding the predator or the predator chasing the prey, see also [36]. The movement of predators controlled by prey density is often referred to as prey-taxis [3, 18, 38]. Prey-taxis can either be attractive or repulsive and plays important roles in population aggregation [38]. In

*Corresponding author. m.chapwanya@up.ac.za; Tel.: +27 12 420 2837; Fax.: +27 12 420 3893

particular, the authors in [38] considered the Holling-Tanner predator-prey model with prey-taxis, ratio-dependent functional responses, and an Allee effect to understand the control of prey invasion. The results indicated that without Allee effect and assuming standard functional response, the predator cannot stop the prey.

In addition to prey-taxis, researchers have proposed and investigated several mathematical models involving predator-taxis, see for example the work [37, 2]. In these models, the authors assumed the prey moves away from the direction of the higher predator density. However, instead of advection induced by direct contact between prey and predator, chemical effects such as specific odor, pheromone, and excrement may also influence the mobility of species [39, 2]. In this work, we consider a diffusive predator prey model with predator-taxis. Under this setup, the prey is lured towards the predator through body coloration or some chemical signalling. Of particular interest, the authors in [39] highlighted that this foraging tactic has been largely ignored.

The discussion above summarised spatial independent models, reaction diffusion models with self and cross diffusion. While a lot of work has focused on the qualitative properties of these mathematical models, very few works have considered the numerical aspect of this problem. It is also important to highlight the singularity in the model when prey population goes to zero. This makes the numerical approach challenging. To the best of our knowledge, this is the first time a nonstandard finite difference study on the Holling-Tanner predator-prey with nonlinear predator-taxis is proposed. Due to the nonlinearity nature of these models, several numerical methods have been proposed and used to simulate the different solution properties of the equations. While in most cases integrated solvers such as Matlab's PDEPE have been used [37], here we highlight [3], where the authors designed a finite volume scheme for the resulting system of equations to predict the pattern formation.

The novelty of this paper is twofold. We propose and investigate the Holling-Tanner predator-prey model with nonlinear predator-taxis. Unlike most existing literature, the current model assumes the prey is lured towards the predator. Secondly, for the proposed nonstandard finite difference scheme, we prove dynamic consistence with the continuous spatial free Holling-Tanner predator-prey model. A coupled nonstandard finite difference scheme and finite volume scheme is proposed for the reaction diffusion system. Numerical simulations are provided to support theoretical findings including the existence of patterns.

This paper is organised as follows. We begin in Section 2 where some preliminary results are outlined. The model formulation is presented in Section 3. Here the model is rendered dimensionless, thus reducing the number of parameters. In Section 4, the global existence of classical solutions is established. In Section 5, we begin by summarising the qualitative properties of the continuous Holling-Tanner predator-prey ordinary differential equation. The qualitative properties of the proposed discrete model are presented and verified in this section. Section 6 presents the linear stability analysis of the full Holling-Tanner predator-prey model with nonlinear predator-taxis. Conditions on the existence of both Turing and Hopf instability are discussed. In Section 7 we present some numerical simulations of the full model. We conclude in Section 8.

2 Preliminaries

In this section, we give some preliminary results for the numerical approach adopted in this work. Let $D \subseteq \mathbb{R}^d$ be a domain ($d \geq 1$) and let $g \in C^0(D, \mathbb{R}^d)$ such that

$$\frac{du}{dt} = g(u), \quad u(0) = u_0, \tag{2.1}$$

with $u_0 \in \mathbb{R}^d$ and $t > 0$. We assume (2.1) defines a dynamical system on D. The point $\tilde{u}$ is an equilibrium point of (2.1) if $g(\tilde{u}) = 0$. The numerical approximation of $u(t)$ is represented by u^n at time $t_n = n\Delta t$, where $n = 0, 1, \cdots$. A finite difference scheme to (2.1) has the general explicit or implicit structure

$$u^{n+1} = \mathcal{D}_g(\Delta t; u^n; u^{n+1}), \quad u^0 = u(0), \tag{2.2}$$

where $\mathcal{D}_g$ denotes the discrete operator.

Definition 2.1. *A one-step scheme (2.2) is called a nonstandard finite difference scheme if at least one of the following conditions is satisfied:*

- *The classical denominator Δt, of the discrete derivative is replaced by a non-negative function $\phi(\Delta t)$ satisfying the requirement $\phi(\Delta t) = \Delta t + \mathcal{O}([\Delta t]^2)$;*
- *Nonlinear terms that occur in the right-hand side of (2.1) are approximated in a non-local way, e.g., $u^2 \approx u^n u^{n+1}$.*

The power and performance of the nonstandard finite difference scheme can be represented in terms of its qualitative stability or dynamic consistency. A much stronger result is the topological dynamic consistency. Further information can be found in [6, 7], and references there in.

Definition 2.2 ([6])**.** *Assume the solution to a differential equation satisfies some property P. A numerical approximation $F(v^n, \Delta t, \lambda)$, is dynamically consistent with the differential equation if the numerical solutions satisfy P for all values of the involved time step.*

Local stability of fixed points for a discrete system can be investigated using the variational matrix. If the absolute value of all eigenvalues satisfy $|\lambda_i| > 1$, a particular fixed point is unstable, or stable if $|\lambda_i| < 1$ for $i = 1, 2, \cdots$. On the other hand, a fixed point is non-hyperbolic if at least one of the eigenvalues is identically equal to one. For a discrete system in $\mathbb{R}^2$, the following Jury's test gives conditions for local stability.

Lemma 2.1. *Consider the variational matrix $J(u, v) \in \mathbb{R}^2 \times \mathbb{R}^2$. A fixed point (u, v) is locally asymptotically stable if the following conditions hold*

$$(i). \quad 1 - \det(J) > 0, \quad (ii). \quad 1 - trace(J) + \det(J) > 0, \quad (iii). \quad 0 < J_{11} < 1, \ 0 < J_{22} < 1.$$

3 Model formulation

Let $x \in \Omega \subset \mathbb{R}^q$, $(q \geq 1)$, be a simply connected bounded domain and $\partial\Omega$, the surface boundary enclosing Ω. We let $u(x,t)$ and $v(x,t)$ be the density of the prey and the density of the predator, respectively.

The characteristic feature of predator-taxis models is that taxis is incorporated into dispersal terms as an advection term where velocity is proportional to the gradient of the predator density, see for example [35, 37]. The flux of the prey is given by

$$J_u = -D_u \nabla u - \gamma(u,v) u \nabla v,$$

and the flux of the predator is

$$J_v = -D_v \nabla v,$$

where D_u and D_v are positive diffusion coefficients and $\gamma(u,v)$ is the predator-taxis function denoting sensitivity of prey to predation risk. Mathematically, this represents attractive (repulsive) effect if $\gamma(u,v) < 0$ $(\gamma(u,v) > 0)$. Here we assume $\gamma(u,v) = -D_{uv}\varphi(u)$ where D_{uv} is a positive constant. The function $\varphi(u)$ is the predator-tactic sensitivity function satisfying the following general hypothesis:

$\mathcal{H}_1$: $\varphi(u) > 0$ for all u,

$\mathcal{H}_2$: $\varphi'(u) \leq 0$ for all u.

Motivated by the above discussion, in this paper we study the following Holling-Tanner predator-prey model with predator-taxis,

$$\begin{aligned} \frac{\partial u}{\partial t} &= D_u \nabla^2 u - D_{uv} \nabla [u\varphi(u)\nabla v] + ru\left(1 - u/\kappa\right) - vf(u), \\ \frac{\partial v}{\partial t} &= D_v \nabla^2 v + vs\left(1 - hv/u\right), \end{aligned} \tag{3.1}$$

where ∇^2 is the Laplace operator. In addition, r and s are the intrinsic rates of increase, κ is the prey carrying capacity, h is the number of prey required to support one predator at equilibrium and $f(u)$ is the response function. In the absence of the predator, the prey population follows a Logistic growth. In literature, several forms of the response function have been investigated. For example, the Holling type I function, [16], Holling type II function, [30, 14, 25, 19], and Holling type III function, [23, 14]. Throughout this work, we generalise the response function and assume $f(u)$ is a differentiable function satisfying the following conditions: $f(0) = 0$ and

$$f(u) \geq 0, \ f'(u) > 0 \text{ for all } u > 0. \tag{3.2}$$

We nondimensionalise the model by choosing the following scales

$$u \sim \kappa, \quad v \sim \frac{\kappa}{h}, \quad t \sim \frac{1}{r}, \quad x \sim \sqrt{\frac{D_u}{r}}.$$

The dimensionless model is given by

$$\begin{aligned}\frac{\partial u}{\partial t} &= \nabla^2 u - d_{uv}\nabla[u\chi(u)\nabla v] + u\,(1-u) - vf(u),\\ \frac{\partial v}{\partial t} &= d\nabla^2 v + v\eta\,(1-v/u)\,,\end{aligned} \tag{3.3}$$

where

$$d_{uv} = \frac{D_{uv}}{D_u}, \quad d = \frac{D_v}{D_u}, \quad \eta = \frac{s}{r},$$

and we have also chosen $\chi(u) = \kappa\varphi(\kappa u)$. The system is complemented with appropriate initial and Neumann boundary conditions.

4 Existence and uniqueness of solutions

The aim of this section is to establish global existence of classical solutions of the following nonlinear system

$$\begin{cases}\dfrac{\partial u}{\partial t} = u(1-u) - \gamma\dfrac{uv}{u+\delta} + \nabla^2 u - d_{uv}\nabla.(\chi(u)u\nabla v),\\ \dfrac{\partial v}{\partial t} = v\eta\left(1-\dfrac{v}{u}\right) + d\,\nabla^2 v,\\ \dfrac{\partial u}{\partial n} = 0,\ \dfrac{\partial v}{\partial n} = 0,\ \forall x\ \in \partial\Omega,\end{cases} \tag{4.1}$$

with initial conditions $u(x,0) = u^0(x) \geq 0, \quad v(x,0) = v^0(x) \geq 0$. Here, $\Omega \subset \mathbb{R}^2$ is an open bounded set of $\mathbb{R}^q$ with boundary $\partial\Omega$ and $\partial/\partial n$ denoting the derivative with respect to the outer normal of $\partial\Omega$. We will follow the approach in [5, 35] where the authors investigated a spatial model with the avoidance behavior of prey and the cost of anti-predator. To this end, we let $\omega = (u,v)^T$, then problem (4.1) can be written as

$$\begin{cases}\dfrac{\partial \omega}{\partial t} = \nabla\cdot(\mathcal{A}(\omega)\nabla\omega) + \mathcal{F}(\omega), \quad \text{in} \quad \Omega\times(0,+\infty)\\ \mathcal{B}\omega = 0 \quad \text{on} \quad \partial\Omega\times(0,+\infty)\\ \omega(\cdot,0) = \omega_0 \quad \text{in} \quad \Omega,\end{cases} \tag{4.2}$$

where

$$\mathcal{A}(\omega) = \begin{pmatrix}1 & -d_{uv}\varphi(u)u\\ 0 & d\end{pmatrix}, \quad \mathcal{F}(\omega) = \left(u(1-u) - \gamma\frac{uv}{u+\delta}, v\eta\left(1-\frac{v}{u}\right)\right)^T.$$

We begin with some notation. For $p \in [1,\infty)$, we denote by $L^p(\Omega)$, the space of measurable scalar function on Ω for which

$$\|u\|_{L^p(\Omega)} = \left(\int_\Omega |u(x)|^p\,dx\right)^{1/p},$$

for $1 \leq p < \infty$, and $\|u\|_{L^\infty(\Omega)} = \operatorname{ess\,sup}_{x\in\Omega}|u(x)| < +\infty$ for $p = +\infty$. We denote by $H^{k^*}(\Omega)$ the Sobolev space of scalar functions that are in $L^2(\Omega)$ together with their weak derivatives of order less than or equal to $k^* \in N^*$. $H_0^1(\Omega)$ is the Hilbert subspace of $H^1(\Omega)$ made of functions

vanishing on $\partial\Omega$. Fix any $p \in (n, +\infty)$, then $H_p^1(\bar{\Omega}, \mathbb{R}^2)$ is continuously embedded in $\mathcal{C}(\Omega, \mathbb{R}^2)$, and we consider solutions of (4.2) in

$$V := H^1_{p,\mathcal{B}} = \left\{ \omega \in H_p^1(\Omega, \mathbb{R}^2) : \ \frac{\partial \omega}{\partial n} = 0 \text{ on } \partial\Omega \right\}. \tag{4.3}$$

We now have the following result.

Theorem 4.1. *Consider the nonlinear system (4.1). There exists a unique nonnegative solution $(u(x,t), v(x,t)) \in V$ defined on $\Omega \times [0,T]$ satisfying $\omega(\cdot, \omega_0) \in C([0,T), V) \cap C^\infty([0,T) \times \bar{\Omega}, \mathbb{R}^2)$, with T dependent on initial data $\omega_0 \in V$.*

Since the eigenvalues of $\mathcal{A}(\omega)$ are all positive, then problem (4.2) is normally elliptic and the proof of Theorem 4.1 follows from [5, p. 17]. Readers can also consult Lemma 3.1 in [35] for further details.

Lemma 4.1. *Suppose the parameters $d, d_{uv}, \gamma, \delta, \eta$ are strictly positive, and $\Omega \subset \mathbb{R}^q$ is a bounded domain with smooth boundary $\partial\Omega$. Assume $0 < u \leq 1$. If $u_0 > 0$, $v_0 \geq 0$, then the system (4.2) has a unique classical solution that exists globally in time satisfying $u(x,t) > 0$ and $v(x,t) \geq 0$ for all $t \in (0, \infty)$ and $x \in \bar{\Omega}$.*

Proof. We first integrate the u-equation of (3.3) over Ω, we obtain

$$\int_\Omega u_t dx = \int_\Omega \nabla \cdot (\nabla u - d_{uv} u \chi(u) \nabla v)\, dx + \int_\Omega (u(1-u) - v f(u))\, dx.$$

Thus, we have

$$\begin{aligned} \frac{d}{dt}\int_\Omega u(x,t)dx &= \int_{\partial\Omega} (\nabla u - d_{uv}\chi(u) u \nabla v) \cdot n dS + \int_\Omega (u(1-u) - v f(u))\, dx \\ &= \int_\Omega u\,(1-u)\, dx - \int_\Omega v f(u) dx \\ &\leq \int_\Omega u\,(1-u)\, dx \\ &\leq \int_\Omega (1-u)\, dx, \quad \text{since } \ u \leq 1. \end{aligned} \tag{4.4}$$

Define

$$y(t) = \int_\Omega u(x,t)dx, \quad t > 0.$$

Then, we have

$$y'(t) + y(t) \leq 1, \quad \text{for all } \ t > 0.$$

From the Gronwall's Lemma, it follows that

$$y(t) \leq 1 + (y_0 - 1)e^{-t}, \quad \text{for all } \ t > 0.$$

We then obtain that

$$\lim_{t\to\infty} \sup ||u||_{L_1} \leq 1,$$

which shows the boundedness of $||u||_{L_1}$. Similarly, we can show that $||v(\cdot,t)||_{L_1}$ is bounded for all $t \in (0,\infty)$. From system (4.1), the growth of predator is dependent on prey only. That is, it depends only on the availability of the food source, u, which is referred to as 'food pyramid' hypothesis. In [4], it is shown that L_1 uniform boundedness of the solution implies L_∞ uniform boundedness connecting this result with the food pyramid condition. That is, since we have that $v(x,t) \geq 0$ and $\sup_{t\geq 0} \int_\Omega v(x,t)dx < K$, consequently, under the food pyramid condition, then

$$\sup_{t\geq 0} ||v(x,t)||_{L_\infty(\Omega)} \leq K^*,$$

where K^* is a constant dependent on K and $||v(x,0)||_{L_\infty(\Omega)}$. Hence, by Theorem 3.1 in [4], the boundedness of $||v||_{L_1}$ implies the boundedness of $||v||_{L_\infty}$. Thus, we can conclude that the boundedness of solution (u,v) of system (4.1) in L_∞ implies global existence of smooth solutions, by [5]. □

5 Model without diffusion

Neglecting diffusion, the Holling-Tanner predator-prey model is given by

$$\begin{aligned} \frac{du}{dt} &= u\,(1-u) - vf(u), \\ \frac{dv}{dt} &= v\eta\,(1 - v/u)\,. \end{aligned} \tag{5.1}$$

Theorem 5.1. *Consider the linear system (5.1) subject to initial conditions $u(0) = u^0 > 0$ and $v(0) = v^0 > 0$. Assuming $f(0) = 0$ and $f'(u) > 0$ for all $u > 0$, then (5.1) is a dynamical system on the biologically feasible region*

$$\Omega = \left\{(u,v) \in \mathbb{R}^2_+ : u \leq 1, v \leq 1\right\}.$$

The proof of the Lemma is straightforward and will be left to the reader. We refer readers to the work [14], where the authors showed that model (5.1) is mathematically well-posed. However, for the proof, we will need to show that the solution is positive and bounded.

5.1 Qualitative analysis

There are two equilibrium solutions to the system. We see that $(1,0)$ is an equilibrium point which corresponds to the absence of predators with the prey being at its carrying capacity. On the other hand, for $v^* \neq 0$, then $u^* = v^*$ and u^* satisfies

$$1 - u^* - f(u^*) = 0.$$

It is clear that a unique positive equilibrium point (u^*, v^*) exists. In particular, if we define $H(u^*) = 1 - u^* - f(u^*)$, and assuming $f(0) = 0$ and $f'(u) > 0$ for all $u > 0$, we see that $H(0) > 0$, $\lim_{u^*\to\infty} H(u^*) < 0$ and $H'(u^*) < 0$. We summarise this as follows

Proposition 5.1. *Assume the functional response $f(u)$ for system (5.1) satisfies assumptions (3.2). The system admits the following equilibria:*

- *a unique predator-free equilibrium $P^0 = (1, 0)$,*
- *a unique coexistence equilibrium $P^* = (u^*, v^*)$.*

Following the ideas in [14], we generalise the model (5.1) as follows

$$\begin{aligned} \frac{du}{dt} &= u(1-u) - uvp(u), \\ \frac{dv}{dt} &= v\eta\,(1 - v/u)\,, \end{aligned} \tag{5.2}$$

where $f(u) = up(u)$ satisfying (3.2). To investigate the local stability of the equilibria of system (5.2), we consider the Jacobian of the system given by

$$J(u,v) = \begin{pmatrix} 1 - 2u - vp(u) - uvp'(u) & -up(u) \\ \eta\left(\dfrac{u}{v}\right)^2 & \eta\left(1 - \dfrac{2v}{u}\right) \end{pmatrix}. \tag{5.3}$$

We determine the local stability of the predator-free equilibrium by evaluating the Jacobian at P^0 to get

$$J(P^0) = \begin{pmatrix} -1 & -p(1) \\ 0 & \eta \end{pmatrix}.$$

Clearly, the equilibrium P^0 is a saddle point. Evaluating the Jacobian at the coexistence equilibrium gives

$$J(P^*) = \begin{pmatrix} -u^*(u^*p'(u^*) + 1) & -u^*p(u^*) \\ \eta & -\eta \end{pmatrix},$$

where we have used the fact that $u^* = v^*$ at P^*. Hence, P^* is locally asymptotically stable provided

$$u^*(u^*p'(u^*) + 1) + u^*p(u^*) > 0, \quad \text{and} \quad u^*(u^*p'(u^*) + 1) + \eta > 0,$$

corresponding to the conditions $\det(J) > 0$ and $\text{trace}(J) < 0$, respectively. In particular, the necessary conditions for local stability of P^* is that $u^*(u^*p'(u^*) + 1) \geq 0$.

Remark 5.1. *Consider the system of equations (5.1). We see that $(u^*p'(u^*) + 1) + p(u^*) = (u^*p(u^*))' + 1 = f'(u^*) + 1 > 0$, where we have used the fact that $f'(u) > 0$ for all $u > 0$. Hence, the stability of P^* is determined solely by the inequality $\text{trace}(J) < 0$.*

We summarise the results for the stability of the equilibria of (5.2), as also proved in [14], in the following result.

Proposition 5.2. *Consider the nonlinear system (5.2):*

(a) The predator-free equilibrium point P^0 is a saddle point.

(b) If $u^*(u^*p'(u^*) + 1) > 0$, the coexistence equilibrium P^* is locally asymptotically stable.

We highlight the global results on the stability of the positive equilibrium which are outlined in [14]. For our needs, the local results are sufficient to develop a dynamically consistent nonstandard finite difference scheme for the system. This is considered in the next section.

Remark 5.2. *Following the work [14], a direct application of the Poincaré-Bendixon theorem shows that under certain conditions* $(u^*(u^*p'(u^*)+1) \leq 0)$*, the equilibrium* P^* *is an unstable focus. See also [25, Chapter 3] for further details.*

5.2 Numerical scheme

As with all nonlinear differential models, it is important to seek for a numerical scheme that can accurately approximate the solution to the system. In [8], the researchers presented an argument against the use of a forward Euler scheme. In particular, while the scheme preserves all the fixed points, both P^0 and P^* are stable and unstable, respectively, depending on the numerical step size $h = \Delta t$ with both fixed points exhibiting chaotic solutions when the step size is varied. Hence, the dynamics of the system will be derived by the numerical method [20]. In this section we propose the nonstandard finite difference scheme due to their qualitative stability properties, [24, 6]. The proposed formulation will also be used in the construction of a dynamically consistent scheme for the Holling-Tanner predator-prey model with predator-taxis proposed in (3.3).

The sub-equation approach proposed in [24] is used in the construction of nonstandard finite difference scheme of (5.2). In the absence of the predator, the prey equation reduces to a standard Logistic equation whose nonstandard scheme is well documented, see for example [24, 9] and references therein. On the other hand, a dynamically consistent discrete model of the Holling type II term (Michaelis-Menten reaction term) was extensively investigated in the work [10]. Combining these results, we propose the following scheme for (5.2)

$$\begin{aligned} \frac{u^{n+1}-u^n}{\phi(\Delta t)} &= u^n(1-u^{n+1}) - v^n u^{n+1} p(u^n), \\ \frac{v^{n+1}-v^n}{\phi(\Delta t)} &= \eta v^n \left(1 - \frac{v^{n+1}}{u^n}\right), \end{aligned} \tag{5.4}$$

with $\phi(\Delta t) = \dfrac{1-e^{-\eta \Delta t}}{\eta}$ and Δt is the step size.

A remark is necessary regarding the current work and the work in [8]. In [8], the authors considered a uniform state predator-prey model with Beddington–DeAngelis functional response. The functional response is assumed to depend on both the predator and the prey populations. A dynamically consistent scheme with respect to the step size is also presented. On contrary, this work deals with the Holling-Tanner predator-prey model with a general response function dependent on the prey population only. While the current model and the work in [8] are different, the presented numerical approach in (5.4) is generic and applicable to general predator-prey models.

In this section, we will go further to show that the proposed scheme in (5.4) for model (5.1), is dynamically consistent with respect to the step-size, stability and preservation of the equilibrium points. Later in Section 6, we will investigate the spatial effects by introducing

predator-taxis into the model. Numerical simulations will be provided.

The explicit form of (5.4) is given by

$$\begin{aligned} u^{n+1} &= \frac{u^n(1+\phi)}{1+\phi(p(u^n)v^n+u^n)}, \\ v^{n+1} &= \frac{v^n(\eta\phi+1)u^n}{\eta\phi v^n+u^n}. \end{aligned} \tag{5.5}$$

The following result is obvious.

Proposition 5.3. *The nonstandard scheme (5.4) is unconditionally positive, i.e.,*

$$u^n > 0,\ v^n \geq 0 \Longrightarrow u^{n+1} > 0,\ v^{n+1} \geq 0.$$

Clearly, the system (5.4) has an explicit form $z^{n+1} = G(\Delta t; z^n)$ where the function $G = [G^1, G^2]^T : \mathbb{R}^2 \to \mathbb{R}^2$. Setting $z^{n+1} = z^n$, we see that the scheme preserves the same fixed points, $P^0 = (1, 0)$ and $P^* = (u^*, v^*)$ as the continuous model (5.1).

We also notice the following, assuming that $u^n \leq 1$ and $v^n \leq 1$ (see Lemma 5.1), then $u^{n+1} \leq 1$ implies that

$$u^n(1+\phi) \leq 1 + \phi(p(u^n)v^n + u^n).$$

That is, $u^n \leq 1 + \phi v^n p(u^n)$, which is always satisfied. It can also be shown that $v^{n+1} \leq 1$ so that the following result follows.

Theorem 5.2. *The nonstandard finite difference scheme (5.4) is a dynamical system on the biological feasible region Ω of the continuous model.*

The local stability of the fixed points will be investigated through the Jacobian of the system. The Jacobian of the scheme (5.4) is given by

$$J(u,v) = \begin{pmatrix} (1+\phi)\dfrac{(1+\phi p(u)v - \phi uvp'(u))}{(1+\phi(vp(u)+u))^2} & -\dfrac{\phi u(1+\phi)p(u)}{(1+\phi[vp(u)+u])^2} \\ \\ \dfrac{v^2(1+\phi\eta)\eta\phi}{(u+\phi\eta v)^2} & \dfrac{u^2(1+\phi\eta)}{(u+\phi\eta v)^2} \end{pmatrix}. \tag{5.6}$$

The eigenvalues of $J(1,0)$, i.e., the predator-free fixed point, are $1+\eta\phi$ and $\dfrac{1}{1+\phi}$. Hence the predator-free fixed point is unstable which is consistent with the properties of the continuous model. In fact, P^0 is a saddle point. Next, we consider the Jacobian at the co-existence fixed point P^*. This can be simplified to

$$J(u^*,v^*) = \begin{pmatrix} 1 - \dfrac{\phi u^*(1+u^*p'(u^*))}{1+\phi} & -\dfrac{\phi u^* p(u^*)}{1+\phi} \\ \\ \dfrac{\eta\phi}{1+\eta\phi} & \dfrac{1}{1+\eta\phi} \end{pmatrix}, \tag{5.7}$$

where we have used the fact that $u^* = v^*$. Here, for convenience of notation, we define $k_\psi =$

$1+\phi\eta$ and $k_\phi = 1+\phi$. It follows

$$\text{trace}(J(u^*,v^*)) = \frac{k_\phi - \phi u^*[u^*p'(u^*)+1]}{k_\phi} + \frac{1}{k_\psi},$$

and

$$\det(J(u^*,v^*)) = \frac{k_\phi - \phi u^*[u^*p'(u^*)+1] + \phi^2\eta u^* p(u^*)}{k_\psi k_\phi}.$$

Using Lemma 2.1, the first condition simplifies to

$$1-\det(J(u^*,v^*)) = \frac{k_\psi k_\phi - \{k_\phi - \phi u^*[u^*p'(u^*)+1] + \phi^2\eta u^* p(u^*)\}}{k_\psi k_\phi}.$$

That is, for $k_\psi k_\phi > 0$,

$$\begin{aligned} k_\phi(k_\psi - 1) + \phi u^*[u^*p'(u^*)+1] - \phi^2\eta u^* p(u^*) &= \eta\phi k_\phi + \phi u^*[u^*p'(u^*)+1] - \phi^2\eta u^* p(u^*) \\ &= \eta\phi(k_\phi - \phi u^* p(u^*)) + \phi u^*[u^*p'(u^*)+1]. \end{aligned}$$

However, at the fixed point (u^*,v^*), we have $k_\phi - \phi u^* p(u^*) = 1+\phi u^*$, then

$$\eta\phi(k_\phi - \phi u^* p(u^*)) + \phi u^*[u^*p'(u^*)+1] = \eta\phi(1+\phi u^*) + \phi u^*[u^*p'(u^*)+1],$$

which is always positive provided $u^*p'(u^*)+1 \geq 0$ for $u^* > 0$, see Proposition 5.2. The second condition is given by

$$\begin{aligned} &1 - \text{trace}(J(u^*,v^*)) + \det(J(u^*,v^*)) \\ &= 1 - \frac{k_\phi - \phi u^*[u^*p'(u^*)+1]}{k_\phi} - \frac{1}{k_\psi} + \frac{k_\phi - \phi u^*[u^*p'(u^*)+1] + \phi^2\eta u^* p(u^*)}{k_\psi k_\phi} \\ &= 1 - \frac{k_\psi k_\phi - k_\psi\phi u^*[u^*p'(u^*)+1] + k_\phi}{k_\psi k_\phi} + \frac{k_\phi - \phi u^*[u^*p'(u^*)+1] + \phi^2\eta u^* p(u^*)}{k_\psi k_\phi} \\ &= \frac{\phi^2\eta u^* p(u^*) + \phi u^*[u^*p'(u^*)+1](k_\psi - 1)}{k_\psi k_\phi} \\ &= \frac{\phi^2\eta u^* p(u^*) + \eta\phi^2 u^*[u^*p'(u^*)+1]}{k_\psi k_\phi} > 0, \end{aligned}$$

using Proposition 5.2. Next we consider $J_{22} = \dfrac{1}{1+\eta\phi}$. Clearly $0 < J_{22} < 1$ for $\eta > 0$ and $\phi > 0$. Finally, we consider $J_{11} = 1 - \dfrac{\phi u^*(1+u^*p'(u^*))}{1+\phi}$ and we need to show that $0 < J_{11} < 1$. Clearly $J_{11} < 1$. In addition, we write

$$J_{11} = 1 - \frac{\phi u^*(1+u^*p'(u^*))}{1+\phi} = \frac{(1+\phi) - \phi u^* - \phi u^{*2}p'(u^*)}{1+\phi} = \frac{1+\phi(1-u^*) - \phi u^{*2}p'(u^*)}{1+\phi},$$

which is always positive since $p'(u^*) \leq 0$ and $0 < u^* \leq 1$. We have the following result

Proposition 5.4. *Consider the discrete system (5.4):*

(a) The predator-free fixed point P^0 is a saddle point.

(b) If $u^*(u^*p'(u^*)+1) > 0$, the coexistence fixed point P^* is locally asymptotically stable.

Clearly, the dynamics of the nonstandard finite difference scheme is consistent with the dynamics of the continuous problem for any step size Δt. In the next section, we formulate a corresponding discrete model for the Holling-Tanner predator-prey model with predator-taxis. The poor performance of standard methods, due to the existence of multiple ghost fixed points, is well documented in the literature, see for example [10]. In this work, the nonstandard finite difference scheme (5.4) will be crucial in the construction of the coupled finite volume and nonstandard finite difference scheme in Section 6.2.

6 The reaction-diffusion model

We recall the predator-prey model with predator-taxis as given in (3.3). For convenience in the analysis, we rewrite the system in the form

$$\begin{aligned} \frac{\partial u}{\partial t} &= f(u,v) + \nabla^2 u - d_{uv}\nabla\cdot(\chi(u)u\nabla v), \\ \frac{\partial v}{\partial t} &= g(u,v) + d\,\nabla^2 v. \end{aligned} \tag{6.1}$$

Without diffusion, the following generalised result holds.

Theorem 6.1. *Assume $f_u + g_v < 0$ and $f_u g_v - f_v g_u > 0$ hold, then the steady state (u^*, v^*) of system (6.1) is stable in the absence of diffusion.*

Remark 6.1. *Consider the model (5.1). In the current formulation, the result in Theorem 6.1 is equivalent to $u^*(u^*p'(u^*)+1) > 0$.*

6.1 Linear stability analysis

Turing instability requires that the stable homogeneous steady state is driven unstable by the interaction of the dynamics and diffusion of the species. The two conditions in Theorem 6.1 will play a crucial role in establishing when Turing instability can form. The following linear stability analysis will be performed around the coexistence equilibrium (u^*, v^*). We assume a perturbed solution of the prey and predator is given by

$$u(z,t) = u^* + \varepsilon\bar{u}(z,t) \quad \text{and} \quad v(z,t) = v^* + \varepsilon\bar{v}(z,t), \tag{6.2}$$

respectively, where $0 < \varepsilon \ll 1$ is a small parameter and $(\bar{u}, \bar{v})$ holds the space and time variation of the perturbation.

Theorem 6.2. *Assume $f_u + g_v < 0$ and $f_u g_v - f_v g_u > 0$ hold, the steady state (u^*, v^*) of system (6.1) loses stability if and only if $g_u d_{uv}\chi(u^*)u^* + f_u d + g_v > 0$, and $(g_u d_{uv}\chi(u^*)u^* + f_u d + g_v)^2 - 4d(f_u g_v - f_v g_u) > 0$, holds.*

Proof. Taylor series expanding system (6.1) at (u^*, v^*) and neglecting higher order terms gives

the following linearised system

$$\begin{aligned}\frac{\partial \bar{u}}{\partial t} &= f_u(u^*, v^*)\bar{u} + f_v(u^*, v^*)\bar{v} + \nabla^2\bar{u} - d_{uv}\chi(u^*)u^*\nabla^2\bar{v},\\ \frac{\partial \bar{v}}{\partial t} &= g_u(u^*, v^*)\bar{u} + g_v(u^*, v^*)\bar{v} + d\,\nabla^2\bar{v}.\end{aligned} \tag{6.3}$$

System (6.3) can be written as the matrix form:

$$\frac{\partial \omega}{\partial t} = J\omega + D\nabla^2\omega, \tag{6.4}$$

where $\omega = (\bar{u}, \bar{v})^t$, denotes vector solutions to the linear system in (6.3), and

$$J = \begin{pmatrix} f_u & f_v \\ g_u & g_v \end{pmatrix}, \ \omega = \begin{pmatrix} \bar{u} \\ \bar{v} \end{pmatrix}, \text{ and } \ D = \begin{pmatrix} 1 & -d_{uv}\chi(u^*)u^* \\ 0 & d \end{pmatrix}. \tag{6.5}$$

Using the standard approach, see for example, [12, 22], we seek for an analytical solution to the linear system (6.3) using seperation of variables in the general form $\omega = e^{ikz+\lambda t}$. This leads to the dispersion relation, which gives an eigenvalue λ as a function of the wave number k, i.e.,

$$\lambda^2 - a(k^2)\lambda + b(k^2) = 0, \tag{6.6}$$

where the trace and the determinant of the Jacobian in (6.5) are given by

$$a(k^2) = (f_u + g_v) - (1 + d)k^2,$$

and

$$b(k^2) = dk^4 - (g_u d_{uv}\chi(u^*)u^* + f_u d + g_v)k^2 + f_u g_v - f_v g_u,$$

respectively. The trace and the determinant provide key conditions for the homogeneous solution to be linearly stable - and more importantly, establishing when Turing instability may occur. The eigenvalues are found from

$$\lambda_k = \frac{a(k^2) \pm \sqrt{a(k^2)^2 - 4b(k^2)}}{2}, \tag{6.7}$$

see Fig. 1(b). When $a(k^2) < 0$ and $b(k^2) > 0$ is always satisfied, we have both roots of equation (6.6) having negative real parts, thus (u^*, v^*) is stable against inhomogeneous perturbations since $\omega \to 0$ as $t \to \infty$. We have $a(k^2) < 0$ always being satisfied since $d > 0$ and $f_u + g_v < 0$. If $b(k^2) < 0$ for some values of $k \neq 0$, then (u^*, v^*) becomes unstable due to inhomogeneous perturbations. Since $d > 0$ and $f_u g_v - f_v g_u > 0$, we might have $b(k^2) < 0$ for some values of $k \neq 0$ when

$$g_u d_{uv}\chi(u^*)u^* + f_u d + g_v > 0.$$

In addition, we are guaranteed that $b(k^2) < 0$ for some values of k if $\min(b(k^2)) < 0$. When

$$k^2_{\min} = \frac{g_u d_{uv}\chi(u^*)u^* + f_u d + g_v}{2d},$$

we have

$$\min(b(k^2)) = -\frac{1}{4d}[(g_u d_{uv}\chi(u^*)u^* + f_u d + g_v)^2 - 4d(f_u g_v - f_v g_u)].$$

Thus, $\min(b(k^2)) < 0$ when

$$(g_u d_{uv}\chi(u^*)u^* + f_u d + g_v)^2 - 4d(f_u g_v - f_v g_u) > 0. \tag{6.8}$$

That concludes the proof. □

Remark 6.2. *The first condition from the previous theorem can be rewritten as*

$$d_{uv} > -\frac{(f_u d + g_v)}{g_u \chi(u^*)u^*}.$$

This can be interpreted as, the only potential destabilizing mechanism of (u^*, v^*) *is presence of a predator-taxis term while predator linear diffusion plays a stabilizing role [32].*

The profile of $b(k^2)$ is dependent on d_{uv}, which plays the role of the bifurcation parameter, see Fig. 1(b). The condition for the marginal stability at some $k = k_c$ is $\min(b(k^2)) = 0$ [29]. We can express $\min(b(k^2)) = 0$ as

$$E_k d_{uv}^2 + F_k d_{uv} + G_k = 0, \tag{6.9}$$

where $E_k = (g_u(u^*)\chi(u^*)u^*)^2$, $F_k = 2g_u\chi(u^*)u^*(f_u d + g_v)$ and $G_k = (f_u d + g_v)^2 - 4d(f_u g_v - f_v g_u)$. For fixed kinetics parameters, the root of equation (6.9) defines a critical predator-taxis coefficient

$$d_{uv}^c = \frac{-F_k \pm \sqrt{F_k^2 - 4E_k G_k}}{2E_k}.$$

Since $d_{uv} > 0$, we let

$$d_{uv}^c = \frac{-F_k + \sqrt{F_k^2 - 4E_k G_k}}{2E_k}.$$

This critical predator-taxis coefficient has the critical wave number

$$k_c^2 = \sqrt{\frac{f_u g_v - f_v g_u}{d}}.$$

Remark 6.3. *In system (6.1), if* $u^*(u^*p'(u^*) + 1) > 0$ *and* $d_{uv} > d_{uv}^c$, *we have* $\min(b(k^2)) < 0$. *This is shown in Fig. 1(b), where we have chosen the response function as the Holling type II function* $p(u) = \dfrac{\gamma}{\delta + u}$.

Remark 6.4. *In system (6.1), when* $u^*(u^*p'(u^*)+1) > 0$ *and* $d_{uv} > d_{uv}^c$ *we have Turing modes. Also, the number of these modes increases as* d_{uv} *is increased. This is shown in Fig.* **??** *with* $p(u) = \dfrac{\gamma}{\delta + u}$.

From the linear stability analysis we can conclude that, if $u^*(u^*p'(u^*) + 1) > 0$ holds in the kinetic model and the system (6.1) then (u^*, v^*) is stable under the kinetic system and is unstable under the system (6.1) when $d_{uv} > d_{uv}^c$. We are also interested in the asymptotic

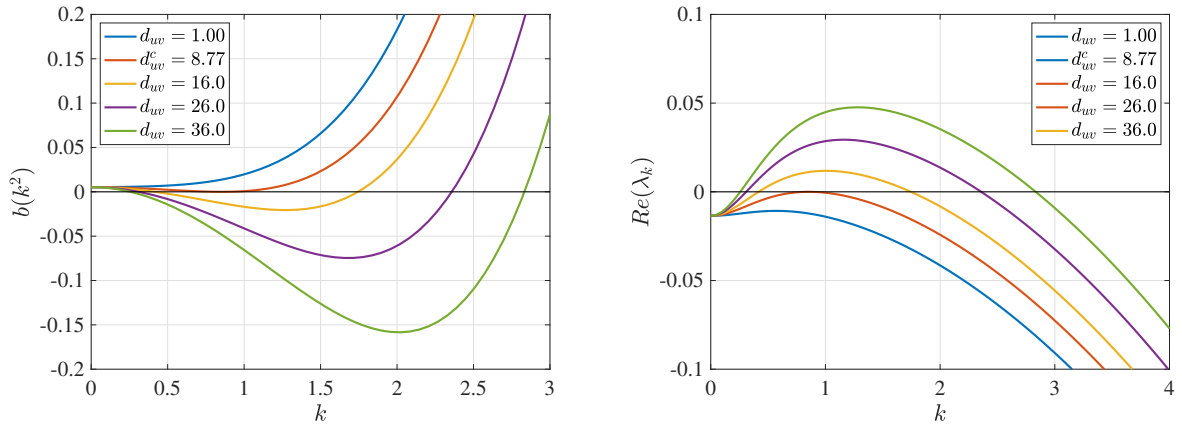

(a) (b)

Figure 1: (a) A plot of $b(k^2)$ for different values of d_{uv}. (b) A plot of the real part of the growth rate of the k^{th} mode for different values of d_{uv}. The parameters are $\delta = 0.8$, $\gamma = 1.00$, $\eta = 0.01$, $d = 0.01$ and $d^c_{uv} = 8.77$.

properties of model (6.1) when $u^*(u^*p'(u^*) + 1) < 0$. In this parameter regime, the model has a oscillations caused by Hopf instability. In Section 7 we investigate numerically the effects of predator-taxis on these oscillations.

6.2 Numerical approximation

In this section, we follow a systematic approach to derive a nonstandard finite difference scheme for the nonlinear predator-taxis system (3.3). We follow the general subequation approach typical of nonstandard finite difference formulations, see for example [24, 11, 1], and references therein. In particular, similar to the present work, the authors in [11] proposed a methodology for constructing unconditionally dynamically consistent nonstandard schemes with respect to positivity for differential models with cross diffusion. The idea was to identify and exploit on the positive (productive) and negative (destructive) terms of the difference scheme. In this section, we develop on these ideas and construct a scheme for the system of equations (3.3) by coupling nonstandard finite difference methods and finite volume methods. We recall $(3.3)_1$, and write

$$\frac{\partial u}{\partial t} = \frac{\partial^2 u}{\partial x^2} - d_{uv}\frac{\partial}{\partial x}\left(u\chi(u)\frac{\partial v}{\partial x}\right) + u(1-u) - uvp(u). \tag{6.10}$$

The scheme for the sub-equation

$$\frac{\partial u}{\partial t} = \frac{\partial^2 u}{\partial x^2} + u(1-u),$$

i.e., the Fishers equation, has attracted the attention of many researchers in the nonstandard finite difference community. Here, we adopt the following scheme as proposed in several works, see for example [24],

$$\frac{1}{\phi(\Delta t)}\left[u_m^{n+1} - u_m^n\right] = \frac{1}{\psi^2(\Delta x)}\left[u_{m+1}^n - 2u_m^n + u_{m-1}^n\right] + u_m^n - \frac{u_m^{n+1}}{3}[u_{m+1}^n + u_m^n + u_{m-1}^n], \tag{6.11}$$

where $\psi(\Delta x) = 2\sin\left(\frac{\Delta x}{2}\right)$ and $\phi(\Delta t) = e^{\Delta t} - 1$ satisfying the asymptotic relations $\psi(\Delta x) = \Delta x + \mathcal{O}(\Delta x^2)$ and $\phi(\Delta t) = \Delta t + \mathcal{O}(\Delta t^2)$, respectively.

First, we will elaborate more on the productive and destructive terms of the predator-taxis. We consider the nonlinear diffusion term $(\chi(u)uv_x)_x$, which we discretise following [11], to get

$$\frac{1}{\psi^2(\Delta x)}\left[\chi(u_m)u_m v_{m+1} - [\chi(u_m)u_m + \chi(u_{m-1})u_{m-1}]v_m + \chi(u_{m-1})u_{m-1}v_{m-1}\right]. \tag{6.12}$$

Combining the schemes (5.4), (6.11) and (6.12), we propose the following scheme for equation $(3.3)_1$,

$$\begin{aligned}\frac{1}{\phi}\left[u_m^{n+1} - u_m^n\right] = u_m^n - \frac{u_m^{n+1}}{3}\left[u_{m+1}^n + u_m^n + u_{m-1}^n\right] - u_m^{n+1}v_m^n p(u_m^n) + \frac{1}{\psi^2}\left[u_{m+1}^n - 2u_m^n + u_{m-1}^n\right] \\ -\frac{d_{uv}}{\psi^2}\left[\chi(u_m^n)u_m^n v_{m+1}^n - [\chi(u_m^n)u_m^n + \chi(u_{m-1}^n)u_{m-1}^n]v_m^n + \chi(u_{m-1}^n)u_{m-1}^n v_{m-1}^n\right].\end{aligned}$$

This scheme has the explicit form

$$\begin{aligned}u_m^{n+1} = &\frac{[u_m^n(1-2\Lambda) + \phi u_m^n + \Lambda(u_{m+1}^n + u_{m-1}^n)]}{(1+\phi\bar{u}_m^n) + \phi p(u_m^n)v_m^n} \\ &+ \Lambda d_{uv}\frac{[\chi(u_m^n)u_m^n + \chi(u_{m-1}^n)u_{m-1}^n]v_m^n}{(1+\phi\bar{u}_m^n) + \phi p(u_m^n)v_m^n} - \Lambda d_{uv}\frac{[\chi(u_m^n)u_m^n v_{m+1}^n + \chi(u_{m-1}^n)u_{m-1}^n v_{m-1}^n]}{(1+\phi\bar{u}_m^n) + \phi p(u_m^n)v_m^n}.\end{aligned}$$

Clearly, the choice $\Lambda = \frac{\phi}{\psi^2} = \frac{1}{2}$ will guarantee unconditional positivity of the first two terms on the right hand side of the equal sign. The negative last term can be multiplied by $2u_m^{n+1}/(u_m^{n+1} + u_m^n)$, which approximates the constant 1 as $\Delta t \to 0$. An alternative term like u_m^{n+1}/u_m^n can also be used. Such modifications, in addition to the requirement $\Lambda = 1/2$, will guarantee that the scheme is unconditionally positive. The reader can consult [11] for further details.

As alluded to earlier, in this work we capitalise on the conservative nature of the cross diffusion term and formulate a finite volume approximation to this term. We consider the following sub equation of (6.10),

$$\frac{\partial u}{\partial t} + d_{uv}\frac{\partial}{\partial x}\left(u\chi(u)\frac{\partial v}{\partial x}\right) = 0, \tag{6.13}$$

which takes the form of nonlinear hyperbolic conservation laws, $u_t + f_x = 0$ with a flux, $f = \chi(u)uv_x$. Naturally, this motivates the use of finite volume methods to disretise this equation, see [17]. If we denote the m^{th} grid cell by $\mathcal{C}_m = (x_{m-\frac{1}{2}}, x_{m+\frac{1}{2}})$, then u_m^n will approximate the average over the m^{th} interval at time t^n, i.e.,

$$u_m^n = \frac{1}{\Delta x}\int_{x_{m-1/2}}^{x_{m+1/2}} u(x,t^n)dx = \frac{1}{\Delta x}\int_{\mathcal{C}_m} u(x,t^n)dx,$$

where $\Delta x = x_{m+1/2} - x_{m-1/2}$ is the grid size. Defining $\mathcal{F}$ as the numerical flux function, then it can be shown that the finite volume scheme for the conservation law is

$$u_m^{n+1} = u_m^n - \frac{\Delta t}{\Delta x}\left[\mathcal{F}(u_m^n, u_{m+1}^n) - \mathcal{F}(u_{m-1}^n, u_m^n)\right],$$

where, considering (6.13), we have

$$\mathcal{F}(u_m^n, u_{m+1}^n) = d_{uv}\chi(u_{m+1/2}^n)u_{m+1/2}^n \frac{v_{m+1}^n - v_m^n}{\Delta x}.$$

A similar construction is given for $\mathcal{F}(u_{m-1}^n, u_m^n)$. The numerical flux has a physical interpretation that the conserved quantity flows from one grid cell to the neighbouring cells at some rate proportional to to the difference between values at either end of a cell. With this formulation in mind, we propose the following coupled nonstandard - finite volume scheme

$$\begin{aligned}\frac{1}{\phi}\left[u_m^{n+1} - u_m^n\right] = u_m^n - \frac{u_m^{n+1}}{3}\left[u_{m+1}^n + u_m^n + u_{m-1}^n\right] - u_m^{n+1}v_m^n p(u_m^n) + \frac{1}{\psi^2}\left[u_{m+1}^n - 2u_m^n + u_{m-1}^n\right] \\ -\frac{d_{uv}}{\psi^2}\left[\chi(u_{m+1/2}^n)u_{m+1/2}^n\left(v_{m+1}^n - v_m^n\right) - \chi(u_{m-1/2}^n)u_{m-1/2}^n\left(v_m^n - v_{m-1}^n\right)\right],\end{aligned}$$

where we have replaced the classical denominator Δx with the non-negative function $\psi(\Delta x)$. As discussed earlier, we will also choose $\Lambda = 1/2$.

Next we recall the model

$$\frac{\partial v}{\partial t} = d\frac{\partial^2 v}{\partial x^2} + v(1 - \frac{v}{u}),$$

i.e., differential model $(3.3)_2$. Assuming u is known and fixed, we see that this is the Fisher equation. Following the nonstandard finite difference scheme above, we obtain the following scheme

$$\frac{1}{\varphi}\left[v_m^{n+1} - v_m^n\right] = \eta v_m^n - \eta\frac{v_m^{n+1}}{3u_m^{n+1}}\left[v_{m+1}^n + v_m^n + v_{m-1}^n\right] + \frac{d}{\psi^2}\left[v_{m+1}^n - 2v_m^n + v_{m-1}^n\right],$$

where $\varphi(\Delta t) = \dfrac{e^{\eta\Delta t} - 1}{\eta}$ satisfying $\varphi(\Delta t) = \Delta t + \mathcal{O}(\Delta t^2)$. The term u is approximated at level $n+1$, assuming the so called Gauss-Seidel approach. We rewrite the scheme in its explicit form to get

$$v_m^{n+1} = \frac{u_m^{n+1}[v_m^n(1 - 2\Upsilon d) + \varphi\eta v_m^n + \Upsilon d(v_{m+1}^n + v_{m-1}^n)]}{u_m^{n+1} + \varphi\eta\bar{v}_m^n}, \tag{6.14}$$

where $\Upsilon = \varphi/\psi^2$ is a constant and $\bar{v}_m^n = \dfrac{v_{m+1}^n + v_m^n + v_{m-1}^n}{3}$. Furthermore, taking $\Upsilon = \frac{1}{2}d^{-1}$ we obtain

$$v_m^{n+1} = \frac{u_m^{n+1}[\varphi\eta v_m^n + \frac{1}{2}(v_{m+1}^n + v_{m-1}^n)]}{u_m^{n+1} + \varphi\eta\bar{v}_m^n}, \tag{6.15}$$

and clearly this scheme replicates positive solutions irrespective of the values of the time and space step sizes. To summarise, the coupled nonstandard finite difference and finite volume scheme for system (3.3) is given by

$$\begin{aligned}u_m^{n+1} &= \frac{\phi u_m^n + \frac{1}{2}(u_{m+1}^n + u_{m-1}^n)}{(1 + \phi\bar{u}_m^n) + \phi v_m^n p(u_m^n)} \\ &\quad - \frac{\frac{1}{2}d_{uv}\left[\chi(u_{m+1/2}^n)u_{m+1/2}^n\left(v_{m+1}^n - v_m^n\right) - \chi(u_{m-1/2}^n)u_{m-1/2}^n\left(v_m^n - v_{m-1}^n\right)\right]}{(1 + \phi\bar{u}_m^n) + \phi v_m^n p(u_m^n)}, \\ v_m^{n+1} &= \frac{u_m^{n+1}[\varphi\eta v_m^n + \frac{1}{2}(v_{m+1}^n + v_{m-1}^n)]}{u_m^{n+1} + \varphi\eta\bar{v}_m^n},\end{aligned} \tag{6.16}$$

where $\bar{u}_m^n = \dfrac{u_{m+1}^n + u_m^n + u_{m-1}^n}{3}$. In the next section we provide several numerical simulations to support our study.

7 Numerical simulations

In this section, we will perform 1D numerical simulations of nonlinear system (3.3) using scheme (6.16). The spatial domain is fixed on $\Omega = (0, 20)$. We will focus on the behaviour of the interior equilibrium $P^* = (u^*, v^*)$ since both populations exist simultaneously. The system undergoes a Hopf bifurcation at P^* when $u^*(u^*p'(u^*) + 1) = 0$. When $u^*(u^*p'(u^*) + 1) > 0$, the direction of Hopf bifurcation is sub-critical and super-critical when $u^*(u^*p'(u^*) + 1) < 0$. Unless otherwise stated, in all the simulations we assume $\chi(u) = 1 - u$ representing the volume filling effect, see [35] and the references there in. We will also use the Holling type II functional response, i.e., $f(u) = \dfrac{\gamma u}{\delta + u}$. All simulations are based on the bifurcation diagram in Fig. 2 with the model parameters selected as follows: $\gamma = 1.0$, $\eta = 0.01$ and $d = 0.01$. The broken line shows the Hopf curve and the solid line shows the Turing curve. Above the Hopf curve is the subcritical region where stable spatial homogeneous solution (left hand side of the solid line), or stable spatial patterns (right hand side of the solid line) are expected. Below the broken line is the supercritical region.

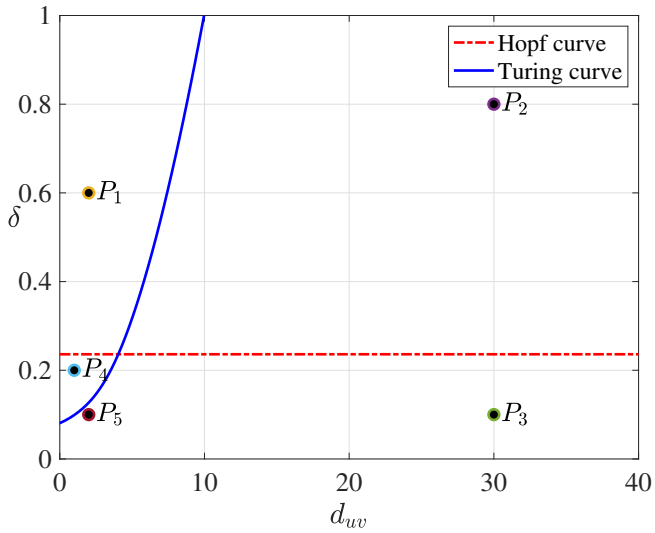

Figure 2: Bifurcation diagram for model in the d_{uv}–δ space.

In all our numerical simulations, we assume periodic boundary conditions. The initial condition is a small random perturbation of the homogeneous steady state (u^*, v^*). We will also run the simulations until they show a behaviour that does not seem to change with time.

When performing numerical simulations, each grid point adds a degree of freedom to the system and the more degrees of freedom the more accurate the solutions are. However, each degree of freedom increases solving time. We will balance size and solve time for scheme (6.16) by performing a mesh convergence analysis. In the analysis we will plot solutions of scheme (6.16) in the sub-critical region of Hopf bifurcation with $d_{uv} = 30$ using mesh sizes $M = 70$,

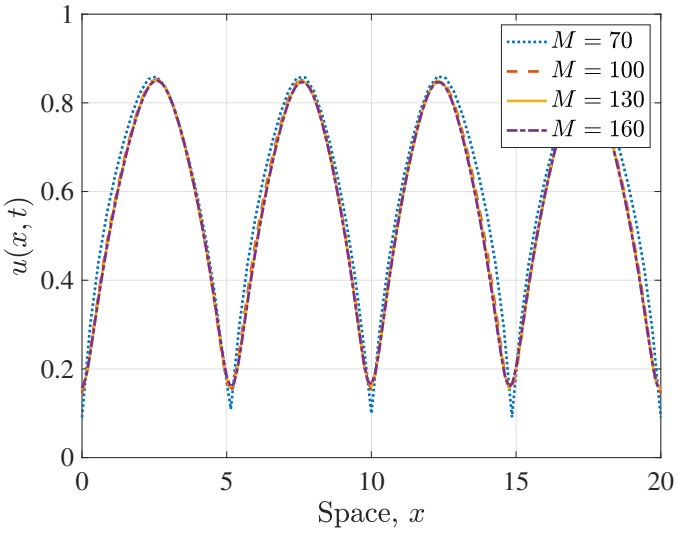

Figure 3: Solution profile for $u(x,t)$ in the sub-critical region for different mesh sizes, corresponding to point P_1 of Fig. 2.

$M = 100$, $M = 130$ and $M = 160$. This analysis will determine the mesh size required to ensure that the simulation results are not affected by changing the size of the mesh.

In Fig. 3 we observe that, when using mesh size $M = 120$ simulation results of scheme (6.16) are not affected by decreasing the mesh size. Thus, this mesh size is used for all our simulations. All simulations were obtained in less than 123 seconds of CPU time on a standard 2.0GHz Quad Core i5 laptop. We also highlight that no meaningful results were obtained using the standard finite difference methods for grid size up to $M = 150$. For the simulations in Fig. 3, different initial perturbation is used and we observe that the initial conditions have no effect on steady-state solutions.

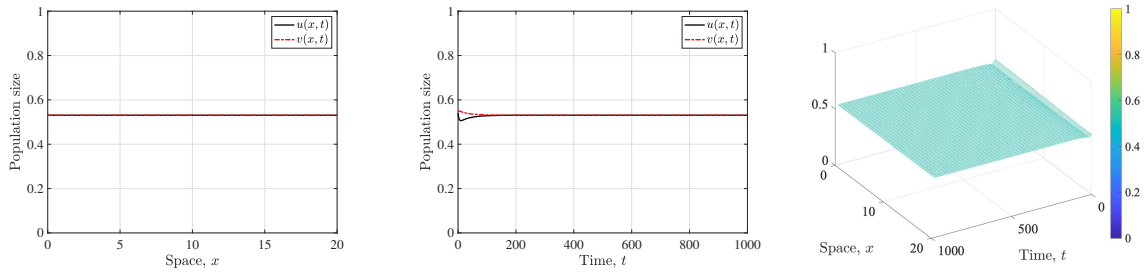

(a) (b) (c)

Figure 4: Simulations in the subcritical region with $d_{uv} = 2.0$ and $\delta = 0.6$, corresponding to point P_1 of Fig. 2. Figure (a) is a solution profile at $t = 1000$ and figure (b) is a solution profile at $x = 10$. We observe no patterns since $d_{uv} < d_{uv}^c = 8.768$.

Simulation results in Fig. 4 and Fig. 5 provide clear evidence that in the sub-critical region of Hopf bifurcation, Turing patterns may appear in the model (3.3) when the effect of predator-taxis is larger than the predator-taxis critical value. In this parameter regime, the unique positive equilibrium is given by $(u^*, v^*) = (0.580, 0.580)$, satisfying $u^*(u^*p'(u^*)+1) = 0.403 > 0$. We observe that if $d_{uv} < d_{uv}^c$, planar solutions are observed, see Fig. 4. On the other hand,

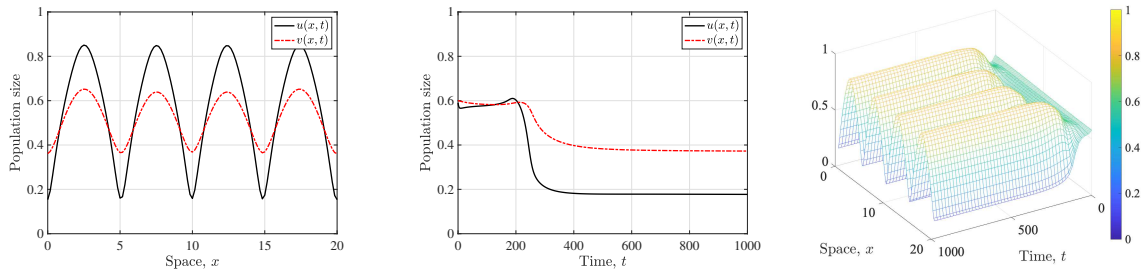

(a) (b) (c)

Figure 5: Simulations in the subcritical region with $d_{uv} = 30$ and $\delta = 0.8$, corresponding to point P_2 of Fig. 2. Figure (a) is a solution profile at $t = 1000$ and figure (b) is a solution profile at $x = 10$. We observe Turing patterns since $d_{uv} > d_{uv}^c = 8.768$.

in support of Theorem 6.2, Fig. 5 shows that the positive equilibrium $(u^*, v^*) = (0.580, 0.580)$ is unstable for $d_{uv} > d_{uv}^c$, and we predict Turing patterns for the predator and prey in model (3.3). It is clear that the regions of higher predator and prey concentration coincide, which highlights the luring mechanism introduced in the model.

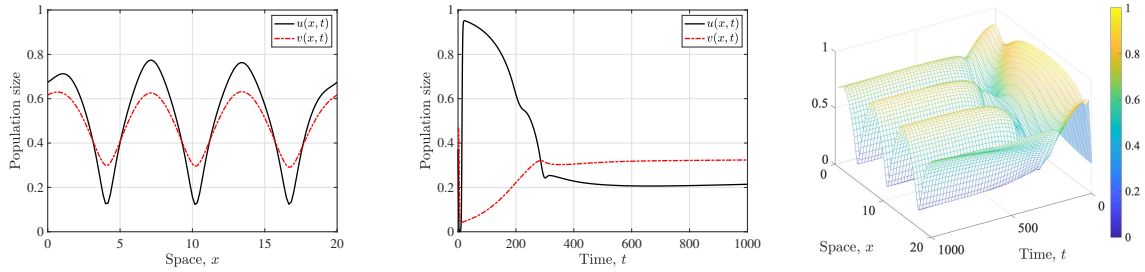

(a) (b) (c)

Figure 6: Simulations in the supercritical region with $d_{uv} = 30$ and $\delta = 0.1$, corresponding to point P_3 of Fig. 2. Figure (a) is a solution profile at $t = 1000$ and figure (b) is a solution profile at $x = 10$. Stationary Turing patterns are observed in this parameter regime.

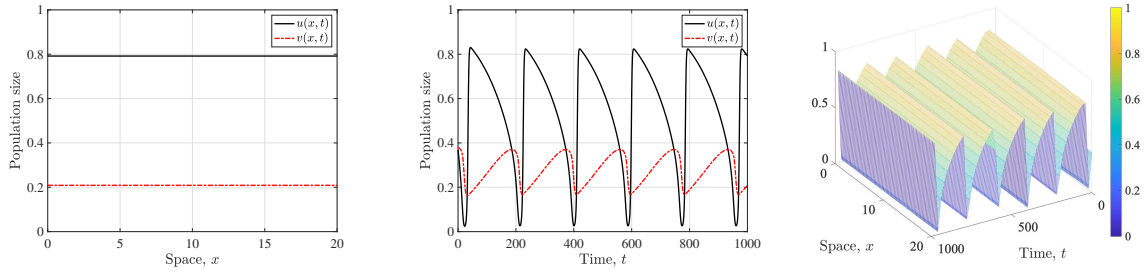

(a) (b) (c)

Figure 7: Simulations in the supercritical region with $d_{uv} = 1.0$ and $\delta = 0.2$, corresponding to point P_4 of Fig. 2. Figure (a) is a solution profile at $t = 1000$ and figure (b) is a solution profile at $x = 10$. Oscillations are observed in this parameter regime.

We also perform simulations in the super-critical region of Hopf bifurcation. In this parameter regime $(u^*, v^*) = (0.358, 0.358)$, satisfying $u^*(u^* p'(u^*) + 1) = -0.0536 < 0$. From numerical simulations, also supported by Figs. 6, 7 and 8, we observe oscillatory solutions. A

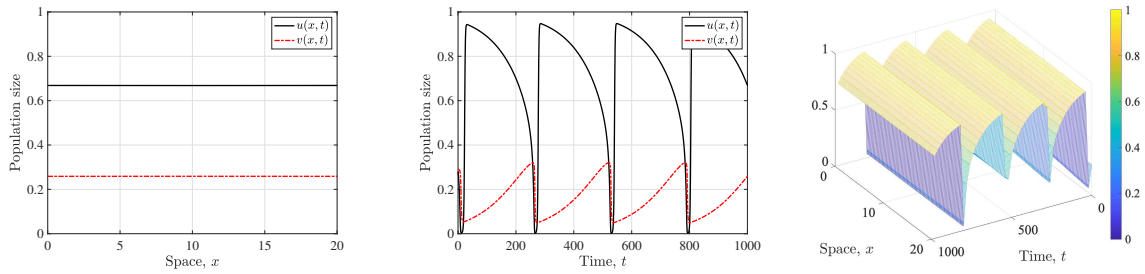

(a) (b) (c)

Figure 8: Simulations in the supercritical region with $d_{uv} = 6.0$ and $\delta = 0.1$, corresponding to point P_5 of Fig. 2. Figure (a) is a solution profile at $t = 1000$ and figure (b) is a solution profile at $x = 10$. Oscillations are observed in this parameter regime.

comparison of simulations in Figs. 4 – 8 predicts one of the following stable states: spatially homogeneous steady state, bulk oscillations, oscillating patterns or stationary Turing patterns. These numerical simulations are entirely consistent with our theoretical results in Theorem 6.2.

8 Conclusions

In this paper, we presented a theoretical and numerical investigation of the Holling-Tanner model with predator-taxis. Predators are assumed to move randomly in their habitat at the same time luring the prey. First the global existence of classical solutions for the proposed model is established. We then design a dynamically consistent nonstandard finite difference scheme for the corresponding spatially homogeneous Holling-Tanner predator-prey model. Choosing the predator-taxis coefficient d_{uv} as the bifurcation parameter, we established conditions for Turing pattern formation using linear stability analysis. A coupled nonstandard finite difference and finite volume scheme that support the qualitative behaviour of the continuous model is derived. Clearly the results in Fig. 3 support the fast convergence properties of the designed scheme. Numerical simulations are provided to explore the spatiotemporal patterns generated by the scheme in the different parameter regimes identified in the analysis. It is observed that Turing patterns appear when the coefficient of predator-taxis term is larger than the critical value d_{uv}^c.

It is worth noting that our methods do apply to a wide class of Holling-Tanner predator-taxis systems with general functional responses. It is important to check that the amplitude of the morphogen pattern is physiologically relevant. Hence, in future, a weakly nonlinear analysis to determine the amplitude of the Turing patterns will be considered. In addition, simulations in higher dimensions will be provided.

Acknowledgements:

The authors acknowledge the support of the South African DSI-NRF SARChI Chair in Mathematical Models and Methods in Bioengineering and Biosciences. MC acknowledge the support, in part, of the DSI-NRF Centre of Excellence in Mathematical and Statistical Sciences (CoE-MaSS), South Africa. The authors thank the anonymous reviewers for their fruitful comments that greatly improved the initial manuscript.

References

[1] A. A. Aderogba and M. Chapwanya. An explicit nonstandard finite difference scheme for the Allen–Cahn equation. *Journal of Difference Equations and Applications*, 21(10):875–886, 2015.

[2] I. Ahn and C. Yoon. Global solvability of prey–predator models with indirect predator-taxis. *Zeitschrift für angewandte Mathematik und Physik*, 72(1):1–20, 2021.

[3] B. E. Ainseba, M. Bendahmane, and A. Noussair. A reaction–diffusion system modeling predator–prey with prey-taxis. *Nonlinear Analysis: Real World Applications*, 9(5):2086–2105, 2008.

[4] N. D. Alikakos. An application of the invariance principle to reaction-diffusion equations. *Journal of Differential Equations*, 33(2):201–225, 1979.

[5] H. Amann. Dynamic theory of quasilinear parabolic equations. ii. reaction-diffusion systems. *Differential and Integral Equations*, 3(1):13–75, 1990.

[6] R. Anguelov and J. M.-S. Lubuma. Contributions to the mathematics of the nonstandard finite difference method and applications. *Numerical Methods for Partial Differential Equations: An International Journal*, 17(5):518–543, 2001.

[7] R. Anguelov, J. M.-S. Lubuma, and M. Shillor. Dynamically consistent nonstandard finite difference schemes for continuous dynamical systems. In *Conference Publications*, volume 2009, page 34. American Institute of Mathematical Sciences, 2009.

[8] N. Bairagi and M. Biswas. A predator-prey model with Beddington-DeAngelis functional response: a non-standard finite-difference method. *Journal of Difference Equations and Applications*, 22(4):581–593, 2016.

[9] M. Chapwanya, O. Jejeniwa, A. R. Appadu, and J.-S. Lubuma. An explicit nonstandard finite difference scheme for the FitzHugh–Nagumo equations. *International Journal of Computer Mathematics*, 96(10):1993–2009, 2019.

[10] M. Chapwanya, J. M.-S. Lubuma, and R. E. Mickens. Nonstandard finite difference schemes for Michaelis–Menten type reaction-diffusion equations. *Numerical Methods for Partial Differential Equations*, 29(1):337–360, 2013.

[11] M. Chapwanya, J. M.-S. Lubuma, and R. E. Mickens. Positivity-preserving nonstandard finite difference schemes for cross-diffusion equations in biosciences. *Computers & Mathematics with Applications*, 68(9):1071–1082, 2014.

[12] G. Gambino, M. C. Lombardo, and M. Sammartino. Turing instability and traveling fronts for a nonlinear reaction–diffusion system with cross-diffusion. *Mathematics and Computers in Simulation*, 82(6):1112–1132, 2012.

[13] C. S. Holling. The components of predation as revealed by a study of small-mammal predation of the European pine sawfly. *The Canadian Entomologist*, 91(5):293–320, 1959.

[14] S.-B. Hsu and T.-W. Huang. Global stability for a class of predator-prey systems. *SIAM Journal on Applied Mathematics*, 55(3):763–783, 1995.

[15] J. Lee, T. Hillen, and M. Lewis. Continuous traveling waves for prey-taxis. *Bulletin of Mathematical Biology*, 70(3):654–676, 2008.

[16] P. Leslie and J. Gower. The properties of a stochastic model for the predator-prey type of interaction between two species. *Biometrika*, 47(3/4):219–234, 1960.

[17] R. J. LeVeque. *Finite volume methods for hyperbolic problems*, volume 31. Cambridge university press, New York, 2002.

[18] C. Li, X. Wang, and Y. Shao. Steady states of a predator–prey model with prey-taxis. *Nonlinear Analysis: Theory, Methods & Applications*, 97:155–168, 2014.

[19] X. Li, W. Jiang, and J. Shi. Hopf bifurcation and Turing instability in the reaction–diffusion Holling–Tanner predator–prey model. *IMA Journal of Applied Mathematics*, 78(2):287–306, 2013.

[20] X. Liu and D. Xiao. Complex dynamic behaviors of a discrete-time predator–prey system. *Chaos, Solitons & Fractals*, 32(1):80–94, 2007.

[21] A. J. Lotka. Relation between birth rates and death rates. *Science*, 26(653):21–22, 1907.

[22] A. Madzvamuse, H. S. Ndakwo, and R. Barreira. Cross-diffusion-driven instability for reaction-diffusion systems: analysis and simulations. *Journal of Mathematical Biology*, 70(4):709–743, 2015.

[23] J. Maynard-Smith. *Models in ecology*. CUP Archive, 1978.

[24] R. E. Mickens. *Nonstandard finite difference models of differential equations*. World Scientific, Singapore, 1994.

[25] J. D. Murray. *Mathematical biology: I. An introduction*, volume 17. Springer Science & Business Media, 2007.

[26] M. L. Rosenzweig and R. H. MacArthur. Graphical representation and stability conditions of predator-prey interactions. *The American Naturalist*, 97(895):209–223, 1963.

[27] M. Solomon. The natural control of animal populations. *The Journal of Animal Ecology*, pages 1–35, 1949.

[28] Y. Song and X. Tang. Stability, steady-state bifurcations, and Turing patterns in a predator–prey model with herd behavior and prey-taxis. *Studies in Applied Mathematics*, 139(3):371–404, 2017.

[29] X.-K. Sun, H.-F. Huo, and H. Xiang. Bifurcation and stability analysis in predator–prey model with a stage-structure for predator. *Nonlinear Dynamics*, 58(3):497, 2009.

[30] J. T. Tanner. The stability and the intrinsic growth rates of prey and predator populations. *Ecology*, 56(4):855–867, 1975.

[31] Y. Tao. Global existence of classical solutions to a predator–prey model with nonlinear prey-taxis. *Nonlinear Analysis: Real World Applications*, 11(3):2056–2064, 2010.

[32] E. Tulumello, M. C. Lombardo, and M. Sammartino. Cross-diffusion driven instability in a predator-prey system with cross-diffusion. *Acta Applicandae Mathematicae*, 132(1):621–633, 2014.

[33] V. Volterra. Sui tentativi di applicazione delle matematiche alle scienze biologiche e sociali. *Giornale Degli Economisti*, pages 436–458, 1901.

[34] Q. Wang, Y. Song, and L. Shao. Nonconstant positive steady states and pattern formation of 1D prey-taxis systems. *Journal of Nonlinear Science*, 27(1):71–97, 2017.

[35] X. Wang and X. Zou. Pattern formation of a predator-prey model with the cost of anti-predator behaviors. *Mathematical Biosciences & Engineering*, 15(3):775, 2018.

[36] Y.-X. Wang and W.-T. Li. Spatial patterns of the Holling–Tanner predator–prey model with nonlinear diffusion effects. *Applicable Analysis*, 92(10):2168–2181, 2013.

[37] S. Wu, J. Wang, and J. Shi. Dynamics and pattern formation of a diffusive predator–prey model with predator-taxis. *Mathematical Models and Methods in Applied Sciences*, 28(11):2275–2312, 2018.

[38] L. Zhang and S. Fu. Global bifurcation for a Holling–Tanner predator–prey model with prey-taxis. *Nonlinear Analysis: Real World Applications*, 47:460–472, 2019.

[39] S. Zhang, H.-L. Chen, K.-Y. Chen, J.-J. Huang, C.-C. Chang, D. Piorkowski, C.-P. Liao, and I.-M. Tso. A nocturnal cursorial predator attracts flying prey with a visual lure. *Animal Behaviour*, 102:119–125, 2015.